Caspian Journal of Environmental Sciences
Online ISSN: 1735-3866
Print ISSN: 1735-3033

Performance evaluation of Artificial Neural Network, Support Vector Machine and Integrated Spectral Indices in satellite image classification

Arash Mesri, Fatemeh Rahimi-Ajdadi*, Iraj Bagheri

Department of Biosystems Engineering, Faculty of Agricultural Sciences, University of Guilan, Guilan, Iran

* *Corresponding E-mail address: rahimi_a@guilan.ac.ir*

ABSTRACT

Satellite remote sensing is effectively used for environmental monitoring and change detection for the sustainable development of human society. While several methods exist for classifying satellite images, relatively few studies have focused on comparing these methods, especially considering the dimensional ratio and spatial distribution of the target phenomena. This study evaluates the performance of three classification methods including ANN, SVM, and an integrated approach that simultaneously uses three spectral indices of NDVI, GNDVI and, NDBI. The overall accuracy and kappa coefficient were calculated from the confusion matrix to statistically evaluate the three methods. Considering that statistical parameters are strongly sensitive to the dispersion and spatial distribution of the test points, a visual comparison was performed by overlaying the classified images with corresponding Google Earth imagery. Comparisons were made for several sample areas, which were categorized based on whether the land uses were integrated or scattered. Based on overall accuracy and kappa coefficient, the methods were ranked as SVM (97.36% and 0.9622), integrated spectral indices (94.06% and 0.9136), and ANN (93.42% and 0.9051). The visual comparison confirmed that SVM provided the best overall performance, consistent with the statistical results. Despite its lower overall accuracy, ANN was found more effective method in narrow areas compared to the other methods. Therefore, ANN is only recommended for detecting land uses with high levels of interference/integration with other features like rivers and roads that are surrounded by some other land uses.

keywords: Land use, Landsat image, Supervised classification, Visual comparison.
Article type: Research Article.

INTRODUCTION

Changes in land use/cover, along with the destruction of productive lands, are among the most significant threats to the environment (Ganasri & Ramesh 2016; Rawat *et al.* 2016). Land changes are typically driven by the conversion of natural resources, such as vegetation and agricultural lands, into urban and residential land uses. These changes are typically caused by human activities such as deforestation, urbanization, and excessive grazing. This phenomenon impacts regional climates and leads to significant environmental changes (Rahimi-Ajdadi & Khani 2022). Forests provide a wide range of ecological products and functions, including balancing the carbon cycle, regulating the water cycle, supporting food supply, mitigating climate change, and many other known and unknown benefits (Slee 2007). On the other hand, agriculture is one of the most important economic sectors in countries. This sector plays a crucial role in job creation and food security, contributing significantly to the country's Gross Value Added (GVA; Talukdar *et al*. 2020). The destruction of forests and agricultural lands, along with the reduction of their productive capacity, poses a serious threat to the economic and social well-being of both current and future generations (Haregeweyn *et al.* 2012; Keno & Suryabhagavan 2014). Due to the ongoing changes in land use, timely information about land cover/use, and human activities is vital for decision-making and planning (Knorn *et al.* 2009). The preparation of land use maps using traditional methods, such as land surveying and analog maps, is not feasible on a large scale due to high costs and time constraints (Ghorbani *et al.*

Caspian Journal of Environmental Sciences, Vol. 24 No. 2 pp.451-464 Received: Oct. 16, 2025 Revised: Dec. 20, 2025 Accepted: Feb. 03, 2026
DOI: 10.22124/cjes.2025.9183

Publisher: University of Guilan

2016). Today, satellite imagery and remote sensing techniques are widely used across various sectors, including agriculture, natural resources, and land use mapping, due to their periodic availability, spectral and radiometric diversity, integrated perspective, and digital format (Zhang *et al.* 2007). There are various methods for delineating thematic phenomena and extracting information from land use maps, including supervised and unsupervised classification techniques. Supervised classification is performed based on training samples provided by the user, followed by classification methods such as maximum likelihood, ANN, minimum distance, SVM, and others (Mather & Tso 2016). The unsupervised classification method is carried out without user intervention, with spectral classification based on the mathematical differences in spectral values. Unlike supervised classification, this method is used when the user lacks sufficient information about the study area and is dealing with large volumes of data (Talukdar *et al*. 2020). The spectral indices method is another unsupervised technique, calculated using specific spectral bands. It combines several spectral bands to present data in an optimal and meaningful way. This method provides images with more detailed information compared to standard sensor bands. The spectral indices method offers numerous advantages, including the ability to highlight one or more phenomena, generate new information, simplify the interpretation and processing of satellite images, and improve classification accuracy in the production of thematic maps. Various spectral indices can be used either as intermediate or final products (Xu 2008). Spectral indices have been widely used to investigate vegetation changes (Lunetta *et al.* 2006; Markogianni *et al.* 2013; Gandhi *et al.* 2015), evaluating the expansion of urban areas (Varshney 2013; Sinha *et al*. 2016), managing crop production (Bandyopadhyay *et al.* 2014; Li *et al.* 2019), assessment of agricultural drought (Wu *et al.* 2015; Zambrano *et al.* 2016), investigating spatial-temporal changes in the earth's thermal pattern (Madanian *et al*. 2018) and hydrology (Rokni e*t al.* 2014; Sarp & Ozcelik 2017). According to the literature, one of the disadvantages of supervised classification is its requirement for extensive fieldwork and skilled personnel to provide training samples, making the process time-consuming and labor-intensive (Adjorlolo *et al*. 2012). On the other hand, these classifications are sensitive to factors such as time, plant growth stage, image quality, weather conditions, and cloud cover, requiring repeated collection of training samples (Zhong *et al.* 2011). In most studies, spectral indices are typically applied to specific categories of land cover, as their accuracy tends to decrease significantly with an elevation in the number of classes. For instance, the study by Ramos and Renza (Ramos *et al.* 2018) on vegetation indices demonstrated that NDVI is largely dependent on the percentage change in vegetation cover. By this method, determining a suitable and general threshold is one of the key challenges in the classification process. Most previous studies have directly or indirectly compared supervised classification algorithms against one another (Caruana & Niculescu-Mizil 2006; Jog & Dixit 2016; Toosi *et al.* 2019). A clear research gap exists in the comparison between supervised classification methods and spectral indices. Additionally, when comparing supervised methods, validation is often not conducted in a comprehensive manner. It is typically performed based on a limited number of test points, without considering their spatial distribution or scattering characteristics. In other words, the accuracy of the classification algorithm is evaluated using statistical methods, without regard for the size, extent, or distribution of the test points. This approach is highly sensitive to the spatial distribution of the test points. For example, the placement of test points within a class, whether in the center or near the border (where spectral mixing may occur) can significantly impact accuracy. However, to minimize the effect of spectral interference at borders, users typically select test points located at the center of each class. Accordingly, this study provides a comprehensive evaluation of supervised (ANN, SVM) and unsupervised (an integrated spectral indices approach combining NDVI, GNDVI, and NDBI) classification methods for satellite imagery analysis. Unlike previous studies, this research uniquely incorporates both statistical accuracy metrics (overall accuracy and kappa coefficient) and detailed visual comparison techniques. The visual analysis, in particular, offers deeper insights into the methods' performance in detecting narrow areas and mixed land uses, which are often challenging to classify. This dual-evaluation approach enables a more nuanced understanding of the strengths and limitations of each method, paving the way for improved classification strategies in remote sensing applications.

MATERIALS AND METHODS

Study area

The study area located in Iran, in the central county of Rudsar City, which is the easternmost City of Guilan Province. Rudsar is located in longitude 50° 12' 34" to 50° 22' 30" E and latitude 10" 02' 37° to 32" 12' 37° N and is adjacent to the Caspian Sea from the north and east (Fig. 1).

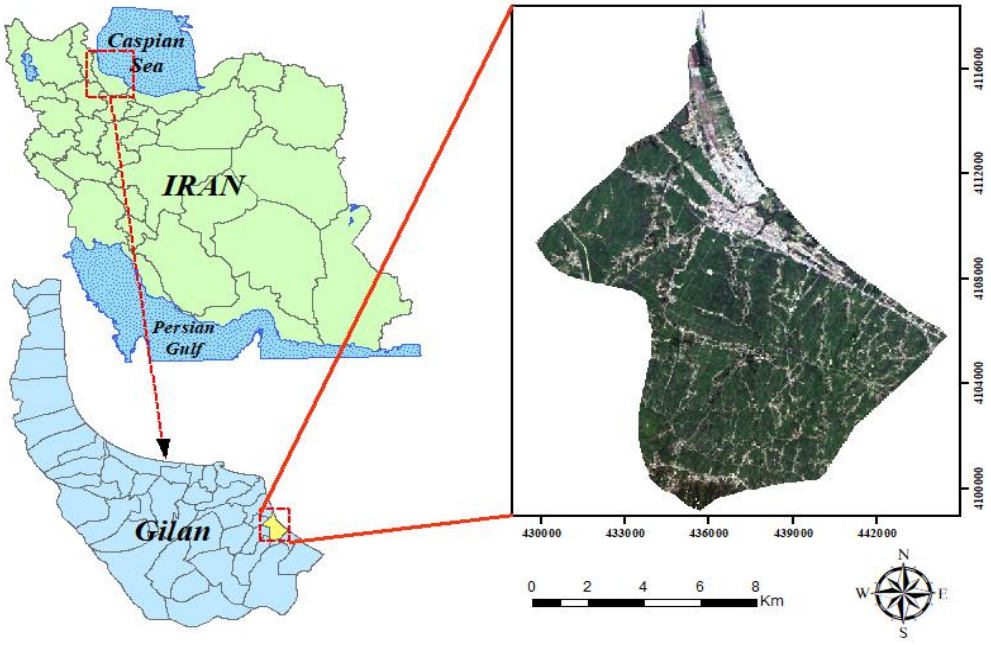

Fig. 1. The location of the study area in Guilan Province, Northwest Iran.

The average annual temperature in the region is 16.5 °C and the average annual precipitation is 1201 mm. The average maximum temperature in the hottest month of the year is July at 25.7 °C and the average minimum temperature in the coldest months of the year is January and February at 1.8 °C. Due to having a humid subtropical climate, Rudsar is one of the best agricultural places in the province and all of the land is covered by vegetation except built-up area and water bodies. The diagram of the work steps is shown in Fig. 2.

Data collection and dataset preparation

The OLI sensor image of Landsat 8 in the year 2020 was used to prepare land use maps of Rudsar (Table 1). The satellite image was obtained from the US Geological Survey website. Due to the importance of proper identification of agricultural land cover in the region, satellite image was used in June (Rahimi-Ajdadi 2022). The image has good conditions including minimal cloud cover prior to image acquisition.

Table 1. Detailed information about the satellite data.

Data Source	Date	Satellite	Sensor	Path	Row	Bands	Resolution
USGS series archive	2020/06/22	Landsat 8	OLI	165	34	11	30 m

Image preprocessing

Atmospheric and radiometric corrections play a crucial role in improving classification accuracy by standardizing spectral values across images. Radiometric correction adjusts pixel intensity to ensure consistent reflectance values, while atmospheric correction removes interference from atmospheric particles such as dust and moisture. These corrections are essential for accurate land use classification, particularly in SVM and spectral index methods, which depend on precise spectral values to differentiate between classes. Without these corrections, spectral distortions can result in misclassification, particularly in areas with variable atmospheric conditions or image quality issues. After performing the radiometric correction, the atmospheric correction was done using QUAC algorithm, which is one of the powerful algorithms for atmospheric correction of multispectral and hyperspectral satellite images (Bernstein *et al*. 2005; Vibhute *et al.* 2015). Geometrical correction was not performed, since the Landsat Level 1 image used already includes radiometric and geometrical corrections through ground control points and a digital elevation model (USGS 2018).

Image classification

ANN and SVM classifiers

The first step in image classification using supervised methods is identifying the different land uses in the studied area. To classify land uses and collect training samples, GPS control points were obtained during field surveys. Additionally, Google Earth images were used to further identify land uses and gather more control

points. Four classes, built-up area, farmland, forest, and water body were considered for Rudsar. Subsequently, 75% of the collected control points were used to classify the satellite images using the SVM and ANN classifiers. ANN classifier simulates and analyses natural phenomena like biological neural networks (human nerve structure) (Dixon & Candade 2008).

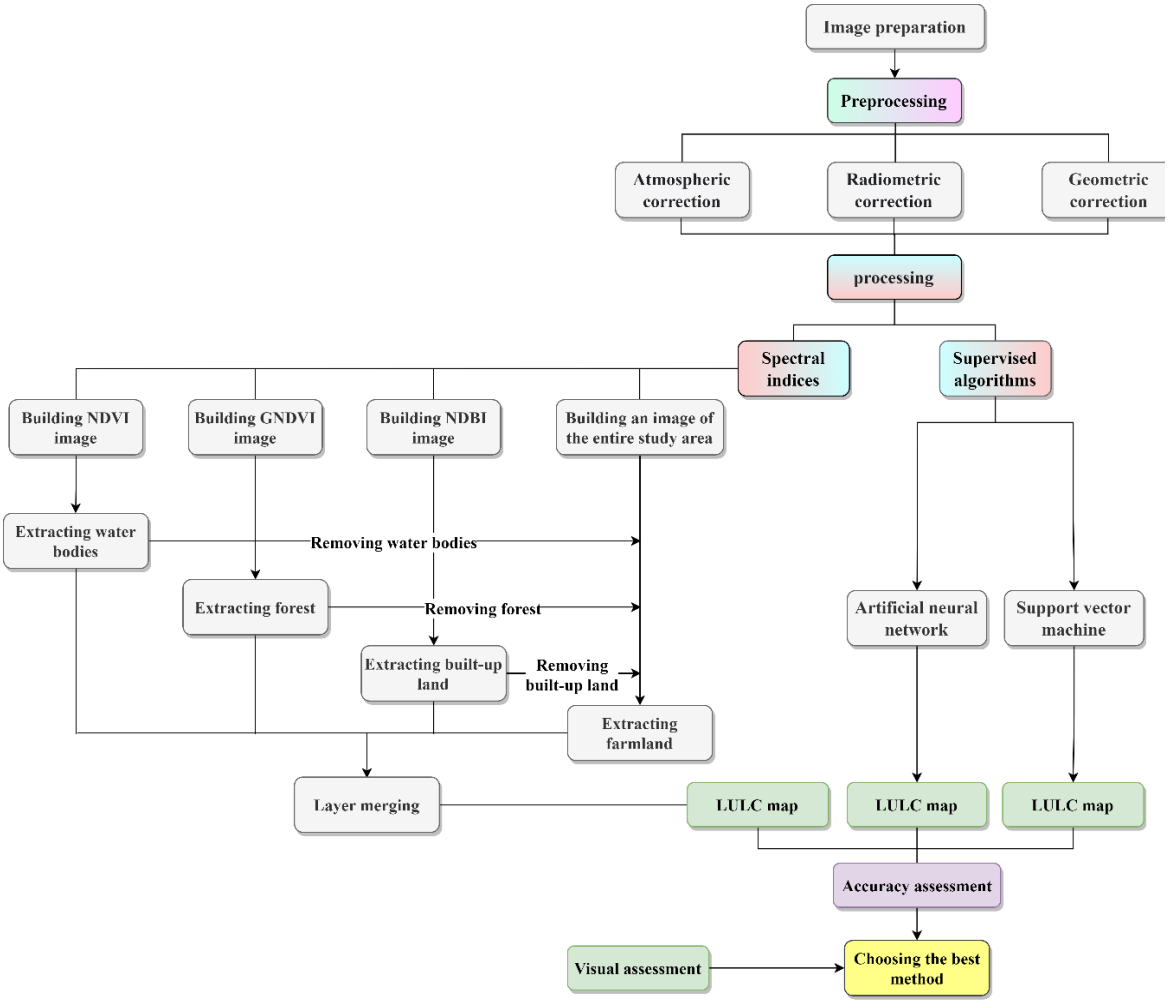

Fig. 2. Methodology of the study.

This model has been the most popular among network classifiers over the past two decades. It exists in several forms, with the multilayer perceptron being the most common (Kotsiantis *et al*. 2007). In an artificial neural network, training samples enter through the input layer and, after being multiplied by the weights of the neurons, are passed to the hidden layers. This process is repeated iteratively, optimizing the weight values and minimizing the error. Due to advantages such as parallel processing, flexibility, and intelligence, ANNs play a crucial role in solving complex problems, including pattern recognition, clustering, modeling, identification, and prediction. While flexible and powerful in handling non-linear relationships, ANNs can be computationally intensive, sensitive to data quality, and prone to overfitting without adequate data. SVM is a non-parametric, supervised statistical method used for classification and regression tasks. Developed based on statistical learning theory in the 1960s, it has demonstrated relatively good performance compared to other methods (Mountrakis *et al*. 2011). The points in SVM can be considered as support vectors that have the smallest distance to the decision boundary. It creates an optimal hyperplane to separate classes by maximizing the margin between them, ideal for high-dimensional data. Increasing the data dimension in this method leads to better results. Specifically, if classes overlap in the spectral space, the data are projected into a higher-dimensional space to improve differentiation. The primary goal of the SVM classification method is to maximize the margin between two classes while minimizing the generalization error as much as possible (Zhang *et al.* 2007). Its limitations include high computational costs, especially with large datasets, and potential overfitting in noisy data.

Integrated spectral indices method

Spectral indices are derived from mathematical calculations involving two or more spectral bands, enabling the identification of specific phenomena. The images generated using spectral indices provide new data that is not present in the original images. This method is computationally efficient but struggles in regions with mixed or narrow land-use areas due to overlapping spectral responses. All the primary mathematical operators can be applied to satellite images; however, division, subtraction, addition, and multiplication are the most commonly used, in that order of priority. In this research, the NDVI, GNDVI, and NDBI indices were utilized to identify and extract water bodies, forests, and built-up areas, respectively. The NDVI, GNDVI, and NDBI indices were selected due to their sensitivity to specific land features. NDVI and GNDVI are responsive to chlorophyll content and are effective for distinguishing different types of vegetation, while NDBI is particularly useful for identifying built-up areas and distinguishing water bodies. It should be mentioned that seasonality plays a crucial role in the effectiveness of spectral indices such as NDVI, GNDVI, and NDBI for land classification. The NDVI and GNDVI indices are sensitive to vegetation growth stages and perform optimally during peak growth seasons, such as spring and summer, when plants exhibit higher reflectance in the near-infrared spectrum. Seasonal fluctuations can cause changes in the values of these indices, and if images are captured during periods of low plant growth, these changes may lead to misclassification. In contrast, NDBI, which is used to detect built-up areas, is less affected by seasonal changes. However, surface conditions, such as variations between wet and dry states, can produce different reflectance values. For this reason, June was selected for data collection in this study to capture the peak vegetation growth period, maximizing spectral differentiation between various areas, including vegetation and built-up regions. This strategic timing minimized the risk of misclassification, particularly in agricultural and forested areas, ultimately enhancing the accuracy of land classification.

NDVI index

The NDVI is used to detect changes in vegetation cover (Knight *et al*. 2006; Guerschman *et al.* 2009; Malik *et al*. 2020). This index is calculated as the difference between the near-infrared (NIR) and red (Red) bands, as shown in Equation 1:

$$\text{NDVI} = \frac{NIR-Red}{NIR+Red} \quad \textbf{(1)}$$

The NDVI values range from -1 to +1. Typically, negative values are associated with water bodies, while values closer to +1 indicate a higher density of vegetation. Rocks and barren soils, which exhibit similar spectral reflectance in the red and NIR bands, usually have values close to zero (Mehta *et al.* 2021).

GNDVI index

The GNDVI (Green Normalized Difference Vegetation Index) is similar to the NDVI, but the green band is used in place of the red band. Compared to the NDVI, the GNDVI exhibits greater sensitivity to chlorophyll (Buschmann & Nagel 1993). The GNDVI is calculated according to Equation 2:

$$\text{GNDVI} = \frac{NIR-Green}{NIR+Green} \quad \textbf{(2)}$$

NDBI index

The NDBI (Normalized Difference Built-up Index) is used to identify urban areas and is derived from two spectral bands: SWIR1 and NIR. The NDBI is calculated as shown in Equation 3:

$$\text{NDBI} = \frac{SWIR1-NIR}{SWIR1+NIR} \quad \textbf{(3)}$$

SWIR1 refers to the shortwave infrared band (Band 6), while NIR to the near-infrared band (Band 5) of the Landsat 8 satellite. The NDBI values range from -1 to +1, where urban built-up areas are represented by positive values. In contrast, vegetation cover yields negative values due to its high reflectance in the near-infrared range.

After completing the pre-processing stage, three maps were generated using each spectral index. A threshold was then defined to extract the desired land use from each index. This threshold is typically determined through trial and error and relies on the user's experience (Sezgin & Sankur 2004). There are also automated methods, such as

Otsu thresholding, which perform thresholding based on statistical information from the image, without requiring user input. A trial-and-error approach is employed to determine the thresholds for these indices, enabling adjustments based on the specific spectral characteristics of the area and local conditions. Since threshold values can be influenced by factors such as seasonal variations and topographic changes, this flexible method allowed for the adaptation of thresholds using prior knowledge of the area, thereby maximizing classification accuracy within this particular geographical context. This approach facilitated optimal separation between land classes and minimized classification errors in areas with similar characteristics.

The steps used for extracting different land use classes are given below:

1. Applying the threshold for NDVI to extract water bodies;
2. Applying the threshold for GNDVI to extract forests;
3. Using logical functions in the image calculator tool to remove mutual pixels of water bodies and forests;
4. Applying the threshold for NDBI to extract built-up lands;
5. Using logical functions in the image calculator tool to remove mutual pixels of water bodies and forests from built-up lands;
6. Using logical functions in the image calculator tool in order to remove water bodies, forests and built-up lands from the entire image resulting in extraction of farmland area;
7. Using mathematical functions in the image calculator tool to merge all four layers/classes and prepare a land use map of Rudsar.

Accuracy assessment

Statistical parameters

Post-classification was conducted to assess how well the classification results align with the actual conditions on the ground (Rahimi-Ajdadi & Khani 2022). For accuracy assessment, a confusion matrix was generated using training and testing data. The overall accuracy, kappa coefficient of agreement, producer's accuracy, and user's accuracy were calculated from the confusion matrix as accuracy criteria (Maryantika & Lin 2017).

The overall accuracy represents the average classification accuracy and is calculated as the ratio of correctly classified pixels to the total number of pixels classified across all classes. The overall accuracy (OA) is computed using Equation 4 (Mather & Tso 2016):

$$OA = \frac{1}{N} \sum_{K=1}^{N} a_{KK} \quad \textbf{(4)}$$

where, N = the total number of classified pixels, and $\sum_{K=1}^{N} a_{KK}$ = the total number of pixels on the main diameter of the confusion matrix (the total number of correctly classified pixels; Richards 1999). The kappa coefficient is another parameter that measures the classification accuracy in comparison to a completely random classification (Mather & Tso 2016). The kappa coefficient (K) is calculated using Equation 5 (Tallón-Ballesteros & Riquelme 2014):

$$K = \frac{N \sum_{i=1}^{r} X_{ii} - \sum_{i=1}^{r} X_{i+} X_{+i}}{N^2 - \sum_{i=1}^{r} X_{i+} X_{+i}} \quad \textbf{(5)}$$

where, N = the total number of ground control points, X_{i+} = the sum of the elements on the i^{th} row, and X_{+i} = the sum of the elements on the j^{th} column. In the confusion matrix, the producer's accuracy, user's accuracy, commission error, and omission error are also provided. The producer's accuracy is calculated as the ratio of correctly classified pixels to the total number of pixels in the corresponding column, while the user's accuracy is determined by the ratio of correctly classified pixels to the total number of pixels in the corresponding row (Ghafari *et al.* 2018). The commission error represents the percentage of pixels that do not belong to the intended class but are incorrectly assigned to it. The omission error refers to the percentage of pixels that originally belonged to the intended class but were incorrectly classified into another class (Alipour *et al.* 2016). To evaluate the accuracy of the classification, GPS control points obtained from field surveys, as well as Google Earth satellite images, were used. For each class, 70% of the pixels were selected as training samples for classification, while the remaining 30% were used as test samples.

Visual assessment

A visual observation was conducted to compare the performance of the SVM, ANN, and integrated spectral indices methods in detecting regions with narrow areas or spatially mixed land uses. First, a boundary for the desired class/land use was drawn in KMZ format using Google Earth Pro software. To minimize error, the Google Earth image closest in time to the satellite image was selected. Given the high resolution of the Google Earth image, the real image and ground reference were considered. This image was then imported into ArcMap, where the land use boundary was carefully delineated using the sketch tool. The boundary created in Google Earth Pro was transferred to ArcMap as a shapefile and used to crop the classification maps generated by the three classification methods. Additionally, the area values corresponding to each region were extracted from the table of content (table of descriptive information) each layer and compared with the real values.

RESULTS AND DISCUSSION

ANN and SVM classifiers

The land use maps classified by ANN and SVM are shown in Fig. 3. It can be observed that farmland covers the largest area compared to other land uses in both classifiers. The soils in the area beside the Caspian Sea have a heavy clay and marsh texture and are predominantly used for rice cultivation, which is the region's primary agricultural crop. Built-up land ranks second in terms of area, with a larger calculated area in the ANN map compared to the SVM map. The results of the accuracy assessment for the ANN and SVM classifiers are presented in Table 2. As shown, the SVM classifier, with an overall accuracy of 97.36% and a kappa coefficient of 0.9622, is more accurate than the ANN classifier, which has an overall accuracy of 93.42% and a kappa coefficient of 0.9051. The highest commission error (15.38%) in the ANN classifier is associated with built-up land, while the highest omission error, 12.50%, is also found in the ANN classification for forests. Previous research has shown that the performance of ANN and SVM classifiers is quite similar, with a slight advantage for SVM (Huang *et al.* 2002; Dixon & Candade 2008; Mokhtari & Najafi 2015).

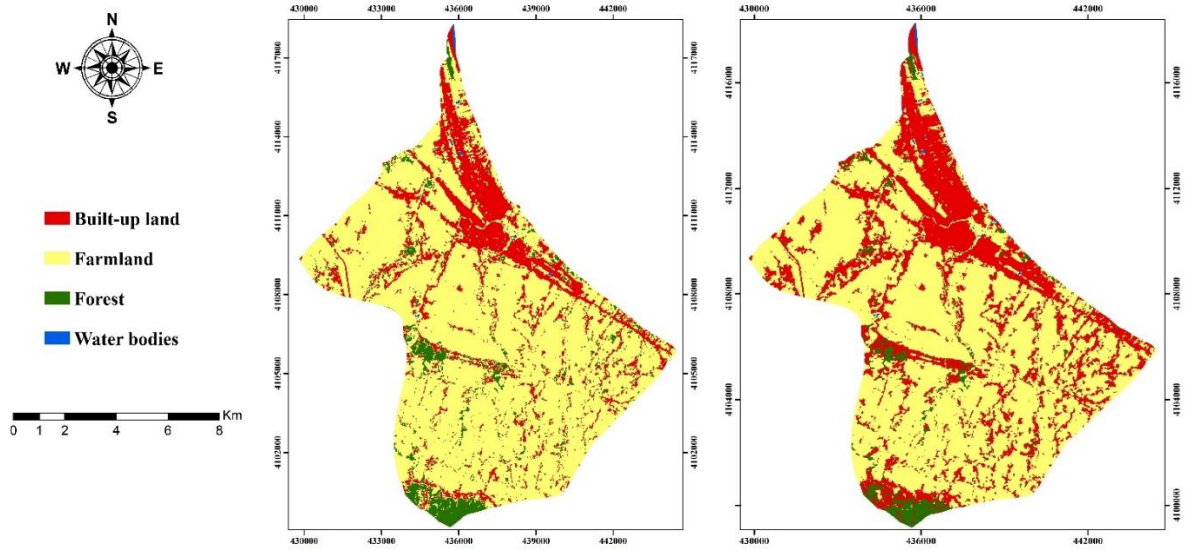

(a) (b)

Fig. 3. land use map of the study area in two different classifiers of a) SVM and b) ANN.

Table 2. Results of accuracy assessment for SVM and ANN classifiers.

	Support Vector Machine				Artificial Neural Network			
	Built-up land	**Farmland**	**Forest**	**Water body**	**Built-up land**	**Farmland**	**Forest**	**Water body**
Commission (%)	1.79	6	0	0	15.38	0	0	0
Omission (%)	0	0	7.50	10	0	8.51	12.50	10
Producer accuracy (%)	100	100	92.50	90	100	91.49	87.50	90
User accuracy (%)	98.21	94	100	100	84.62	100	100	100
Overall accuracy (%)	97.36				93.42			
Kappa coefficient	0.9622				0.9051			

Table 3 compares the areas of different land uses classified by ANN and SVM. According to the table, the area of built-up land in the SVM classification is 2,125.95 ha, while in the ANN classification, this value is 3,279.78 ha, which is 10% higher than that of SVM. The area of farmland classified by SVM is 8,741.14 ha, whereas the corresponding value in the ANN classification is 7,792.88 ha, about 8% less than that of SVM. The results from the accuracy assessment and area comparison of the land uses indicate that ANN has the greatest error in distinguishing farmland from built-up land. In a similar study conducted by Hazini & Hashim (2015), SVM was more accurate than ANN, and ANN exhibited the most error in separating built-up land and vegetation (Hazini & Hashim 2015), that is consistent with our result. Forest has the third place in terms of having the largest area in both classifiers. It should be mentioned that forests have been faced with many changes in the last two decades and deforesting is still ongoing in the studied area.

Table 3. Results of ANN and SVM classifiers in estimating the area of different land uses.

	Support vector machine		**Artificial neural network**	
Class	Area (ha)	Area (%)	Area (ha)	Area (%)
Built-up land	2125.95	18.43	3279.78	28.44
Farmland	8741.14	75.80	7792.88	67.57
Forest	640.20	5.55	415.43	3.60
Water body	25.09	0.22	44.29	0.39

Integrated spectral indices method

The optimal thresholds used for each land use for each index are shown in Table 4.

Table 4. Threshold value of each index in each land use class

Indices	**Type of land use**	**Threshold value**
NDVI	Water body	-1 to -0.2
GNDVI	Forest	0.855 to 1
NDBI	Built-up land	-0.275 to 1

The scattering of agricultural areas, as well as the number of small rice fields, was notably higher than that of other land use classes. This could lead to significant errors in estimating farmland area due to the low spatial resolution of Landsat images (with a pixel size of 900 m²). To improve accuracy in delineating farmland, the farmland area was derived by subtracting the areas of the other three land uses (as classified by the three indices) from the entire study area. The land use map produced using the integrated spectral indices is shown in Fig. 4. Visual observation reveals that, similar to the ANN and SVM classifications, the largest areas are dedicated to farmland, followed by built-up land, forest, and water bodies, respectively. The classified map obtained using the integrated spectral indices method is more similar to the SVM classifier. The overall accuracy and kappa coefficient for the integrated spectral indices method are 94.06% and 0.9136, respectively (Table 5). Farmland has the highest commission error (13.7%), while the highest omission error is associated with forests (14.51%).

Table 5. Results of accuracy assessment in classifying with integrated spectral indices.

	Built-up land	**Farmland**	**Forest**	**Water body**
Commission (%)	2.40	13.7	1.85	0
Omission (%)	1.22	3.07	14.51	10
Producer accuracy (%)	98.78	96.92	85.48	90
User accuracy (%)	97.59	86.30	98.14	100
Overall accuracy (%)	94.06			
Kappa coefficient	0.9136			

Table 6 shows the area of different land uses produced by the integrated spectral indices method. A comparison of the results in Table 6 and Table 3 indicates that the areas of the classes obtained by the spectral indices are very close to those derived from the SVM classifier. The area of built-up land in the spectral indices method (30.72 ha) is 1.424% higher than that of SVM. The area of farmland obtained by the spectral indices method is 8,734.32 ha, which is 0.078% (6.82 ha) less than the SVM result. The area of forest classified by the spectral indices method is 642.96 ha, which is 0.429% (2.76 ha) greater than that of SVM.

Table 6. Results of land use area calculated with the integrated spectral indices method.

Class	**Area (ha)**	**Area (%)**
Built-up land	2156.67	18.68
Farmland	8734.32	75.66
Forest	642.96	5.57
Water body	10.62	0.09

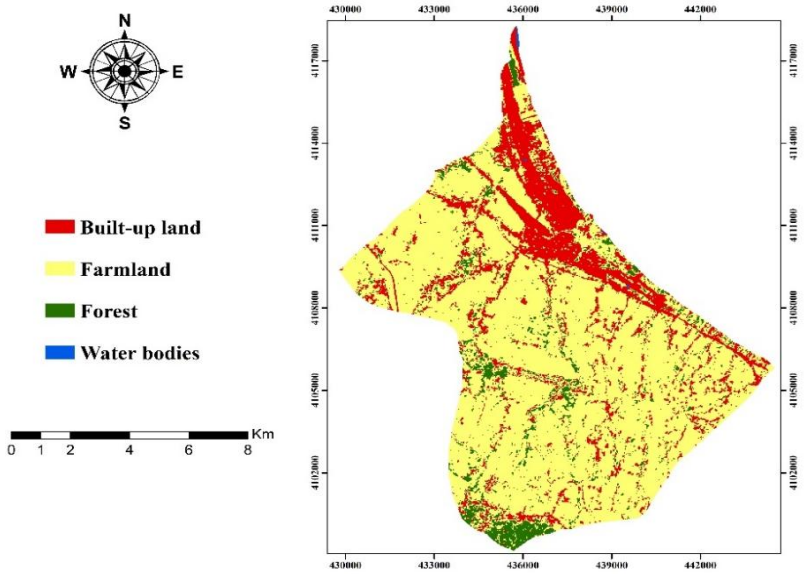

Fig. 4. land use map produced by integrated spectral indices method.

Statistical comparison of three classifiers

Table 7 provides a summary of the accuracy assessment results for the three classification methods. According to the table, the SVM and integrated spectral indices methods achieve higher accuracies than the ANN method. A comparison between SVM and the spectral indices shows that they deliver very similar performance. However, with slightly higher accuracy, SVM demonstrates the best performance among the three methods. When comparing farmland accuracy, SVM achieves the best results with 6% commission error and 0% omission error (Tables 2 and 5). ANN ranks second, with 0% commission error and 8.51% omission error. The highest error in ANN is due to insufficient separation of pixels for built-up land and farmland along their boundaries. The integrated spectral indices method ranks third, with a commission error of 13.7% and an omission error of 3.07%. Most of the farmland error in this method is due to the inseparability between forest and farmland.

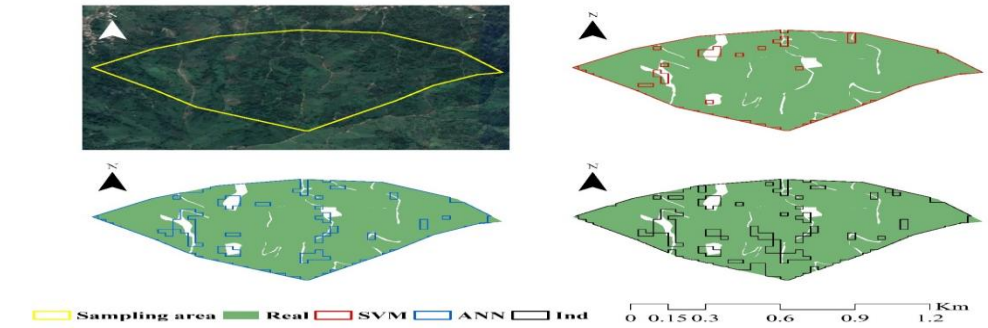

(a)

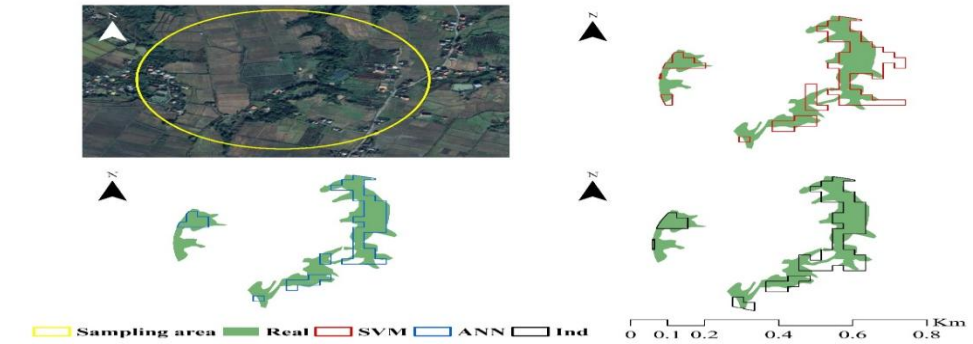

(b)

Fig. 5. Graphical representation of matching forest area obtained by three classification methods with real area: (a) large and concentrated forest area; (b) small and scattered forest area.

Table 7. Overall accuracy and kappa coefficient obtained in SVM, ANN and spectral indices methods.

Type of method	Overall accuracy (%)	Kappa coefficient
Support Vector Machine	97.36	0.9622
Artificial Neural Network	93.42	0.9051
Indices	94.06	0.9136

Visual comparison of three classifiers

The accuracy assessment using the confusion matrix generally evaluates the correspondence between classified pixels and test pixels. The test points are prepared by the users and are highly dependent on the spatial distribution of these points across the region. Additionally, this assessment is conducted without considering the simplicity or complexity of the classification problem, whether it involves separate or mixed land uses. For this reason, in addition to the statistical assessment, visual interpretation was also conducted to further investigate the capabilities and characteristics of the studied classifiers. The visual assessment focused on evaluating the ability of the classifiers to detect discrete or mixed areas. We aimed to determine which classifier performed better in detecting regions with narrow shapes (low width-to-length ratio) or mixed areas. Fig. 5 shows two samples of the forest class. The white areas represent roads that were removed from the forest area. The errors associated with the three methods can be analyzed in two ways: 1) forest pixels that were correctly detected as forest by the different methods; and 2) non-forest pixels (white areas) that were incorrectly classified as forest by the methods. According to Fig. 5a, the ANN classifier visually detects roads and treeless regions better than the other two methods. However, it identifies forests as 2.8961 ha less than the actual area (Table 8). The SVM classifier provides the closest estimate to the real value, with a difference of 2.2818 ha. The high accuracy of SVM aligns with the results of the confusion matrix (statistical accuracy assessment). Similarly, in Fig. 5b, although SVM performs poorly in detecting roads, it provides the closest estimate of the real area, with a difference of 6.9825 ha.

Table 8. The area of two regions of a) Large and concentrated area and b) small and scattered area for each classifier.

		Area (ha)			
Land use		**Real**	**SVM**	**ANN**	**Ind**
Forest	a	80.34	82.62 (2.84%)	77.44 (-3.60%)	73.62 (-8.36%)
	b	8.00	6.98 (-12.75%)	4.39 (-45.12%)	5.94 (-25.80%)
Built-up land	b	6.65	3.33 (-49.92%)	9.54 (43.45%)	3.96 (-40.45%)
Farmland	b	11.36	15.48 (36.22%)	11.52 (1.37%)	18.02 (58.54%)
Water body	a	5.96	2.52 (-57.69%)	3.79 (36.32%)	1.53 (74.35%)
	b	3.66	0 (-100%)	0.54 (-85.24%)	0.18 (-95.08)

The numbers in parenthesis indicate the error percentage in estimating each classifier compared to the actual value. In Fig. 6, the built-up land is visually assessed. The ANN classifier performs the best in detecting scattered and small built-up areas compared to the other classifiers. However, it estimates the built-up area as 2.89 ha larger than the actual value. The integrated spectral indices method provides the closest estimate to the real value, with a difference of 2.69 ha. The ANN method ranks second after the spectral indices in terms of estimated area. Fig. 7 shows a section of farmland located in the urban area. A comparison of the three methods indicates that ANN performs best in identifying the boundaries of farmland. According to Table 8, ANN also provides the closest area estimate to the actual value, followed by the SVM method. Classification errors were primarily observed in areas with mixed land use boundaries, such as agricultural land adjacent to built-up areas. Contributing factors to these errors include spectral similarities between land types, atmospheric interference, and limitations in spatial resolution. For instance, agricultural land pixels near urban areas are sometimes misclassified as built-up due to spectral overlap. Fig. 8 shows a water body with a very low width-to-length ratio and a curved shape. According to Fig. 8a, ANN performs best in detecting river pixels. Among the studied classifiers, it provides the closest estimate to the actual area, with a difference of 2.1636 ha. Fig. 8b further emphasizes that ANN performs best in detecting river areas in mixed land uses where different land uses are intertwined. According to Fig. 8b, SVM is unable to detect the water body. Overall, the results from the visual evaluation indicate that ANN tends to overestimate the boundaries and accounts for more area than the real amount. This characteristic can be considered an advantage for land uses with narrow shapes or areas. In other words, ANN is more effective than the other classifiers in detecting narrow areas, especially when they are surrounded by multiple land uses. However, while ANN excels in these scenarios, SVM generally provides more satisfactory results in detecting broader areas. While visual assessment is valuable for examining the spatial location and boundary accuracy of classifications, it has limitations. It relies on human perception, which can lead to challenges, particularly in areas with complex land use boundaries. Moreover, visual comparison lacks the precision of quantitative analysis and may overlook

subtle errors that statistical measurements can identify. By combining visual assessment with metrics such as overall accuracy and the kappa coefficient, these shortcomings can be addressed, enabling a comprehensive evaluation that captures both qualitative and quantitative aspects of classifier performance.

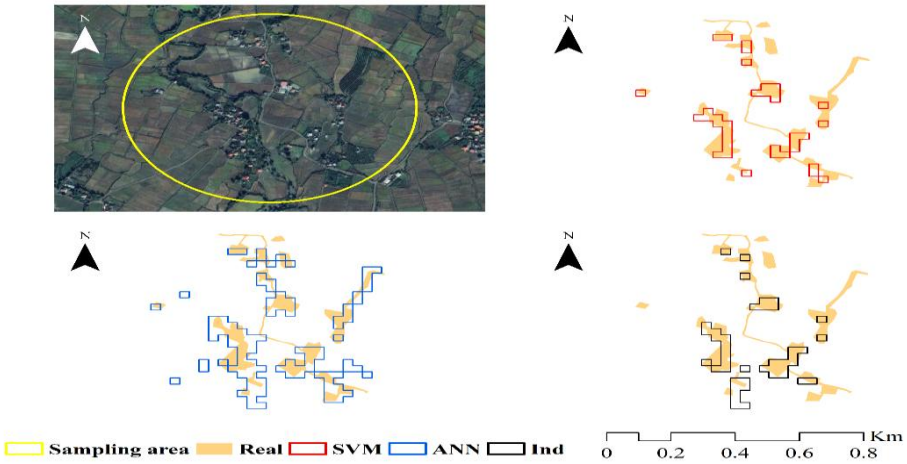

Fig. 6. Graphical representation of matching built-up area obtained by three classification methods with real area.

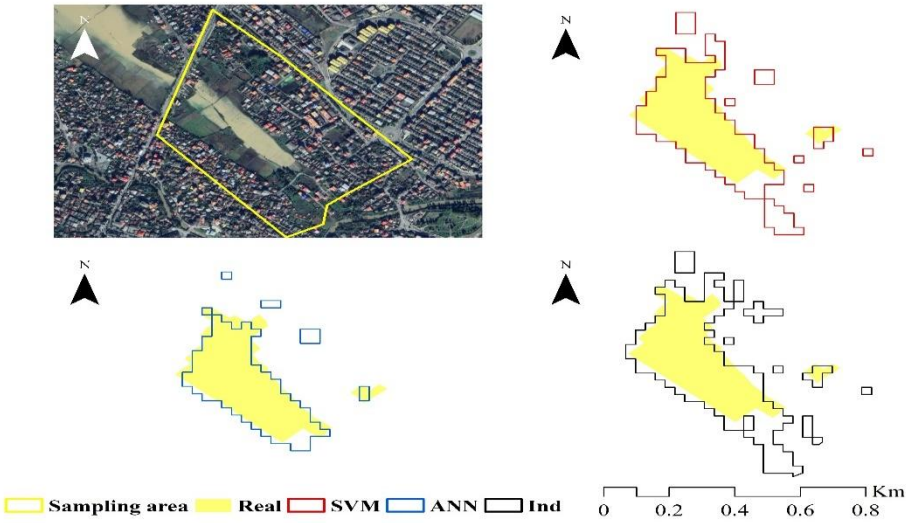

Fig. 7. Graphical representation of matching farmland obtained by three classification methods with real value.

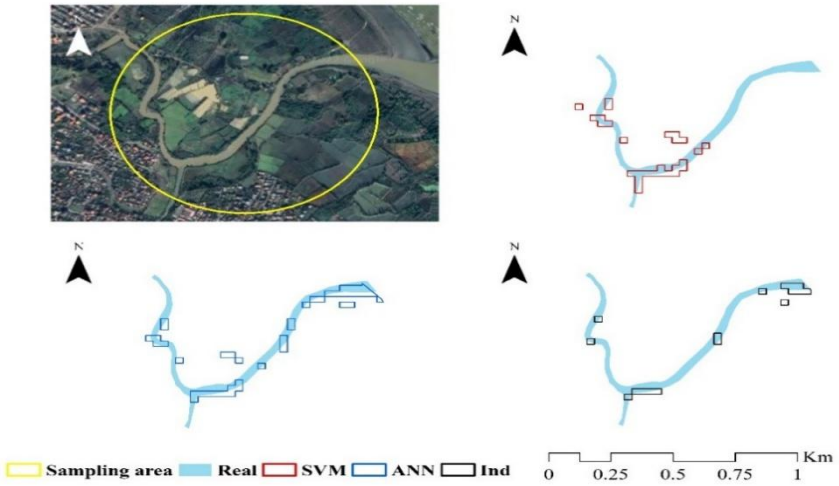

(a)

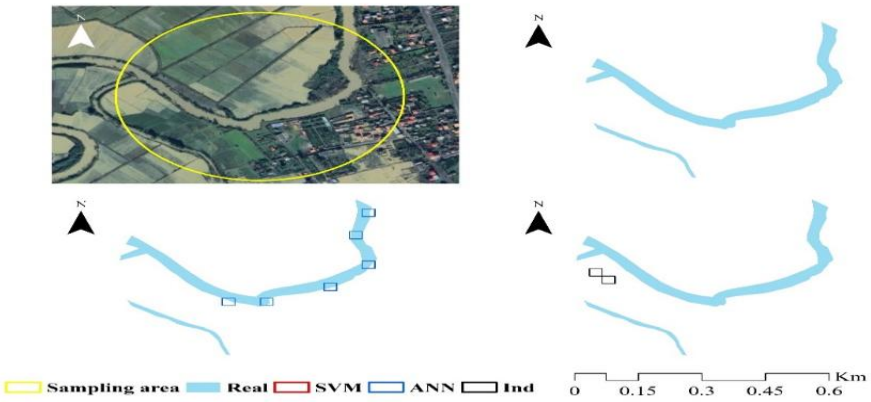

(b)

Fig. 8. Graphical representation of matching water bodies obtained by three classification methods with real value: (a) large and concentrated area; (b) small and scattered area.

CONCLUSION

This study compared the performance of three methods—ANN, SVM, and integrated spectral indices—in classifying land uses. The results from the confusion matrix indicated that SVM is the most powerful classifier for estimating land use areas, followed by the integrated spectral indices method. The results of the visual assessment showed that the ANN classifier is more effective than the others in detecting regions with narrow shapes (low width-to-length ratio), despite its lower overall accuracy. Specifically, when detecting narrow classes, such as rivers or roads, within regions with spatially mixed or intertwined land uses, ANN performs better due to its tendency to overestimate narrow areas. In general, based on both statistical and visual assessments, the integrated spectral indices method provides intermediate performance and offers a suitable estimate of land use areas. Therefore, it can be considered a viable option in situations where field surveying is not feasible, or when time and budget constraints limit such activities.

ACKNOWLEDGMENTS

The authors thank University of Guilan and the Science and Technology Park of Gilan Province for their financial support.

REFERENCES

Adjorlolo, C, Mutanga, O, Cho, M & Ismail, R 2012, Challenges and opportunities in the use of remote sensing for C3 and C4 grass species discrimination and mapping. *African Journal of Range & Forage Science*, 29: 47-61.

Alipour, F, Aghkhani, M, Abasspour-Fard, M & Sepehr, A 2016, Demarcation and estimation of agricultural lands using etm+ imagery data (Case study: Astan Ghods Razavi Great Farm). *Journal of Agricultural Machinery*, 4: 244-254.

Bandyopadhyay, K, Pradhan, S, Sahoo, R, Singh, R, Gupta, V, Joshi, DK & Sutradhar, AK 2014, Characterization of water stress and prediction of yield of wheat using spectral indices under varied water and nitrogen management practices. *Agricultural Water Management*, 146: 115-123.

Bernstein, LS, Adler-Golden, SM, Sundberg, RL, Levine, RY, Perkins, TC, Berk, A, Ratkowski, AJ, Felde, G & Hoke, ML 2005, Validation of the QUick atmospheric correction (QUAC) algorithm for VNIR-SWIR multi-and hyperspectral imagery. In *Algorithms and Technologies for Multispectral, Hyperspectral, and Ultraspectral Imagery XI*, 5806: 668-678.

Buschmann, C & Nagel, E 1993, In vivo spectroscopy and internal optics of leaves as basis for remote sensing of vegetation. *International Journal of Remote Sensing*, 14: 711-722.

Caruana, R & Niculescu-Mizil, A 2006, An empirical comparison of supervised learning algorithms. In Proceedings of the 23rd international conference on Machine learning, pp. 161-168.

Dixon, B & Candade, N 2008, Multispectral landuse classification using neural networks and support vector machines: one or the other, or both? *International Journal of Remote Sensing*, 29: 1185-1206.

Ganasri, B & Ramesh, H 2016, Assessment of soil erosion by RUSLE model using remote sensing and GIS-A case study of Nethravathi Basin. *Geoscience Frontiers*, 7: 953-961.

Gandhi, GM, Parthiban, b, Thummalu, N & Christy, A 2015, NDVI: Vegetation change detection using remote sensing and gis–A case study of Vellore District. *Procedia Computer Science,* 57: 1199-1210.

Ghafari, S, Moradi, HR & Modarres, R 2018, Comparison of object-oriented and pixel-based classification methods for land use mapping (Case study: Isfahan-Borkhar, Najafabad and Chadegan plains). *Journal of RS and GIS for Natural Resources,* 9: 40-57.

Ghorbani, A, Aslami, F & Ahmadabadi, S 2016, Land and use mapping of Kaftareh of watershed of Ardabil using visual and digital processing of etm+ image. *Natural Ecosystems of Iran,* 6: 23-43.

Guerschman, JP, Hill, MJ, Renzullo, LJ, Barrett, DJ, Marks, AS & Botha, EJ 2009, Estimating fractional cover of photosynthetic vegetation, non-photosynthetic vegetation and bare soil in the Australian tropical savanna region upscaling the EO-1 Hyperion and MODIS sensors. *Remote Sensing of Environment,* 113: 928-945.

Haregeweyn, N, Berhe, A, Tsunekawa, A, Tsubo, M & Meshesha, DT 2012, Integrated watershed management as an effective approach to curb land degradation: a case study of the Enabered watershed in northern Ethiopia. *Environmental Management,* 50: 1219-1233.

Hazini, S & Hashim, M 2015, Comparative analysis of product-level fusion, support vector machine, and artificial neural network approaches for land cover mapping. *Arabian Journal of Geosciences.* 8: 9763-9773.

Huang, C, Davis, L & Townshend J 2002, An assessment of support vector machines for land cover classification. *International Journal of Remote Sensing,* 23: 725-749.

Jog, S & Dixit, M 2016, Supervised classification of satellite images. In 2016 Conference on Advances in Signal Processing (CASP) IEEE, 93-98.

Keno, K & Suryabhagavan, K 2014, Multi-temporal remote sensing of landscape dynamics and pattern change in Dire district, Southern Ethiopia. *Journal of Geomatics,* 8: 189-194.

Knight, JF, Lunetta, RS, Ediriwickrema, J & Khorram S 2006, Regional scale land cover characterization using MODIS-NDVI 250 m multi-temporal imagery: A phenology-based approach. *GIScience & Remote Sensing,* 43: 1-23.

Knorn, J, Rabe, A, Radeloff, VC, Kuemmerle, T, Kozak, J & Hostert, P 2009, Land cover mapping of large areas using chain classification of neighboring Landsat satellite images. *Remote Sensing of Environment,* 113: 957-964.

Kotsiantis, SB, Zaharakis, I & Pintelas P 2007, Supervised machine learning: A review of classification techniques. *Emerging Artificial Intelligence Applications in Computer Engineering,* 160: 3-24.

Li, C, Li, H, Li, J, Lei, Y, Li, C, Manevski, K & Shen, Y 2019, Using NDVI percentiles to monitor real-time crop growth. *Computers and Electronics in Agriculture,* 162: 357-363.

Lunetta, RS, Knight, JF, Ediriwickrema, J, Lyon, JG & Worthy, LD 2006, Land-cover change detection using multi-temporal MODIS NDVI data. *Remote Sensing of Environment,* 105: 142-154.

Madanian, M, Soffianian, AR, Koupai, SS, Pourmanafi, S & Momeni, M 2018, The study of thermal pattern changes using Landsat-derived land surface temperature in the central part of Isfahan Province, Iran. *Sustainable Cities and Society,* 39: 650-661.

Malik, S, Pal, SC, Das, B & Chakrabortty, R 2020, Intra-annual variations of vegetation status in a sub-tropical deciduous forest-dominated area using geospatial approach: A case study of Sali watershed, Bankura, West Bengal, India. *Geology, Ecology, and Landscapes,* 4: 257-268.

Markogianni, V, Dimitriou, E & Kalivas, D 2013, Land-use and vegetation change detection in Plastira artificial lake catchment (Greece) by using remote-sensing and GIS techniques. *International Journal of Remote Sensing,* 34: 1265-1281.

Maryantika, N & Lin, C 2017, Exploring changes of land use and mangrove distribution in the economic area of Sidoarjo District, East Java using multi-temporal Landsat images. *Information Processing in Agriculture,* 4: 321-332.

Mather, P & Tso, B 2016, Classification methods for remotely sensed data: CRC press, Florida, US, 357 p.

Mehta, A, Shukla, S & Rakholia, S 2021, Vegetation change analysis using normalized difference vegetation index and land surface temperature in Greater Gir Landscape. *Journal of Scientific Research,* 65: 1-6.

Mokhtari, MH & Najafi, A 2015, Comparison of support vector machine and neural networl classification methods in land use information extraction through Landsat TM data. *Water and Soil Science,* 19: 35-44.

Mountrakis, G, Im, J & Ogole, C 2011, Support vector machines in remote sensing: A review. *ISPRS Journal of Photogrammetry and Remote Sensing*, 66: 247-259.

Rahimi-Ajdadi, F 2022, Land suitability assessment for second cropping in terms of low temperature stresses using landsat TIRS sensor. *Computers and Electronics in Agriculture*, 200: 107205.

Rahimi-Ajdadi, F & Khani, M 2022. Multi-temporal detection of agricultural land losses using remote sensing and gis techniques, Shanderman, Iran. *Acta Technologica Agriculturae*, 25: 67-72.

Ramos, JF, Renza, D & Ballesteros, DM 2018, Evaluation of spectral similarity indices in unsupervised change detection approaches. *Dyna*, 85: 117-126.

Rawat, KS, Mishra, AK & Bhattacharyya, R 2016, Soil erosion risk assessment and spatial mapping using LANDSAT-7 ETM+, RUSLE, and GIS—A case study. *Arabian Journal of Geosciences*, 9: 1-22.

Richards, JA 1999, Remote Sensing Digital Image Analysis. Springer, Berlin, Germany, 494 p.

Rokni, K, Ahmad, A, Selamat, A & Hazini, S 2014, Water feature extraction and change detection using multitemporal Landsat imagery. *Remote Sensing*, 6: 4173-4189.

Sarp, G & Ozcelik, M 2017, Water body extraction and change detection using time series: A case study of Lake Burdur, Turkey. *Journal of Taibah University for Science*, 11: 381-391.

Sezgin, M & Sankur, B 2004. Survey over image thresholding techniques and quantitative performance evaluation. *Journal of Electronic Imaging*, 13: 146-165.

Sinha, P, Verma, NK & Ayele, E 2016, Urban built-up area extraction and change detection of Adama municipal area using time-series Landsat images. *International Journal of Advanced Remote Sensing and GIS*, 5: 1886-1895.

Slee, B 2007, Landscape goods and services related to forestry land use. Presented at Multifunctional Land Use: Meeting Future Demands for Landscape Goods and Services, Berlin, Heidelberg: Springer Berlin Heidelberg, pp. 65-82.

Tallón-Ballesteros, AJ & Riquelme, JC 2014, Data mining methods applied to a digital forensics task for supervised machine learning. In: Computational Intelligence in Digital Forensics: Forensic Investigation and Applications, Springer, pp. 413-428.

Talukdar, G, Sarma, AK & Bhattacharjya, RK 2020, Mapping agricultural activities and their temporal variations in the riverine ecosystem of the Brahmaputra River using geospatial techniques. *Remote Sensing Applications: Society and Environment*, 20: 100423.

Toosi, NB, Soffianian, AR, Fakheran, S, Pourmanafi,S, Ginzler, C & Waser, LT 2019, Comparing different classification algorithms for monitoring mangrove cover changes in southern Iran. *Global Ecology and Conservation*, 19: e00662.

USGS, 2018. Landsat missions. Landsat collection 1. https://www.usgs.gov/landsat-missions/landsat-collection-1#publications: Earth Resources Observation and Science (EROS) Center.

Varshney, A 2013, Improved NDBI differencing algorithm for built-up regions change detection from remote-sensing data: an automated approach. *Remote Sensing Letters*, 4: 504-512.

Vibhute, AD, Kale, K, Dhumal, RK & Mehrotra, S 2015, Hyperspectral imaging data atmospheric correction challenges and solutions using QUAC and FLAASH algorithms. International Conference on Man and Machine Interfacing (MAMI), 1-6.

Wu, D, Qu, JJ & Hao, X 2015, Agricultural drought monitoring using MODIS-based drought indices over the USA Corn Belt. *International Journal of Remote Sensing*, 36: 5403-5425.

Xu, H 2008, A new index for delineating built-up land features in satellite imagery. *International Journal of Remote Sensing*, 29: 4269-4276.

Zambrano, F, Lillo-Saavedra, M, Verbist, K & Lagos, O 2016, Sixteen years of agricultural drought assessment of the BioBío region in Chile using a 250 m resolution Vegetation Condition Index (VCI). *Remote Sensing*, 8: 530.

Zhang, Z, Verbeke, L, De Clercq, E, Ou, X & De Wulf, R 2007, Vegetation change detection using artificial neural networks with ancillary data in Xishuangbanna, Yunnan Province, China. *Chinese Science Bulletin*, 52: 232-243.

Zhong, L, Hawkins, T, Biging, G & Gong, P 2011, A phenology-based approach to map crop types in the San Joaquin Valley, California. *International Journal of Remote Sensing*, 32: 7777-7804.

Bibliographic information of this paper for citing:

Mesri, A, Rahimi-Ajdadi, F, Bagheri, I 2026, Performance evaluation of Artificial Neural Network, Support Vector Machine and Integrated Spectral Indices in satellite image classification. Caspian Journal of Environmental Sciences, 24: 451-464.